Oxidation of Metals, Vol. 34, Nos. 5/6, 1990

On the Oxidation of Iron in CO_2+CO Gas Mixtures: I. Scale Morphology and Reaction Kinetics

Rune Bredesen*,† and Per Kofstad*

Received February 15, 1990

High-purity iron has been oxidized in CO_2 and CO_2+CO gas mixtures and different total gas pressures (0.1-1 atm.) at 1000-1200°C. Reaction rates and kinetics have been studied by thermogravimetry and reacted specimens have been characterized by electron microscopy and x-ray diffraction. The time dependence of the growth of wüstite may generally be described by an S-shaped curve. The scale texture of intially formed wüstite is related to that of the underlying γ-iron; however, as the scale grows, the texture gradually changes to a final one in which the (001) plane of wüstite is parallel to the iron substrate. The oxidation rate increases with this change in texture. It is concluded that the oxidation during these initial stages is essentially controlled by a surface reaction, and that the increasing reaction rate reflects an increased number of reaction sites at the surface during the change in texture. As the scale grows in thickness, the reaction rates go through a maximum, and are followed by a decreasing, parabolic-like behavior, reflecting that iron diffusion through the scales becomes increasingly important. Cold-worked iron oxidizes faster than annealed iron during the initial oxidation stages. An overall model is presented that relates the scale morphology to the detailed reaction kinetics under different reaction conditions.

KEY WORDS: Iron; oxidation in CO_2+CO mixtures; reaction kinetics; scale morphology.

INTRODUCTION

Reaction Kinetics

The initial oxidation of iron at high temperatures leads to formation of films or thin scales of wüstite, $Fe_{1-\delta}O$. The diffusion of iron through wüstite

*Department of Chemistry, P.O. Box 1033 Blindern, 0315 Oslo 3, Norway.
†Permanent address: Senter for Industriforskning, P.O. 124 Blindern, 0314 Oslo 3, Norway.

0030-770X/90/1200-0361$06.00/0

is rapid, and it has been concluded that the initial oxidation is mainly controlled by the reaction at the scale/gas interphase.[1-11] For reactions in gas mixtures of CO_2+CO, it has been proposed that the rate-limiting step either involves dissociation of adsorbed CO_2 or the subsequent incorporation of adsorbed oxygen into the wüstite.[2-4,8,9,12-14]

The main features of the reaction kinetics of oxidation of iron in CO_2+CO gas mixtures are that the reaction rate gradually increases with time to a maximum value (often denoted as the linear stage of scale growth), and on further oxidation the reaction rate decreases and eventually reaches parabolic reaction behavior.

Some investigators have subdivided the initial reaction kinetics in CO_2+CO gas mixtures into two different linear stages.[2,4,5] The reaction rate during the first stage (which in the following is termed film growth) is always lower than that of the second stage (scale growth). It has further been proposed that the scale thickness at the transition between these stages depends on temperature, the CO_2 content in the gas mixture, and the crystal structure of iron.[2,4] For the first linear stage it has also been indicated that the reaction rates depend on the grain size of the iron specimens and that the rates are controlled by dissociation of CO_2 on surfaces of wüstite crystals, which are crystallographically related to the iron substrate. During the second stage, however, the reaction rates are controlled by dissociation of CO_2 on wüstite surfaces, which have a different orientation due to the formation of a growth texture.[5] However, no detailed results have been reported.

Scale Appearance

Previous studies of nucleation of wüstite on iron reacted in low-pressure oxygen indicate that crystallographic relations exist between iron and the wüstite film.[15-19] Furthermore, it has been shown that the density of nuclei and the induction periods for appearance of the nuclei depend on the crystallographic orientation of the surface of α-iron.

Morphological changes of wüstite layers formed during oxidation in oxygen at very low total pressures ($P_{O_2} = 10^{-4}$ atm.) at 1050 and 1200°C have also been studied by continuously observing the surface in a hot stage SEM.[19-21] These studies have shown that for thin wüstite scales, grains coalesce by migration of dislocations (observed as pits on the wüstite surface) from grain boundaries into the crystals; and it was proposed that dislocations with a screw component may form pits on the scale surface with the dislocations emerging at the pit vertices. Wüstite scales on cold-worked iron had more pits in the surface than wüstite scales on annealed

iron. From this it was suggested that dislocations in the wüstite scale are inherited from the metal through an epitaxial metal/oxide interface.

Scales formed in CO_2+CO and H_2O+H_2 gas mixtures after extended periods of reaction have been reported to be adherent and compact, and to consist of large columnar grains which have the (001) plane parallel to the iron surface.[5,7,9]

This paper is a part of an extended study of the reaction behavior of iron in CO_2+CO mixtures at 1000–1200°C and particularly relates kinetics to changes in scale morphology during the initial stages of the reaction.

EXPERIMENTAL

These studies have been performed on rectangular specimens cut from high-purity (99.99+%) iron sheets with thicknesses ranging from 0.125–2 mm. The specimens had total surface areas ranging from 2–8 cm^2. The specimens were polished with emery paper (grade 240–400), then chemically polished in ethanol +30% HCl for about 30 sec, and finally washed with deionized water and ethanol. They were then introduced into the thermogravimetric apparatus and treated in high-vacuum ($<6\times10^{-9}$ atm.) at 120°C for about 15 min. During this treatment, the specimens were degassed and thermally etched. While maintaining high-vacuum, the specimens were lifted out of the hot zone of the furnace and cooled for 15–30 min. Then, the experimental conditions were established and the specimens were lowered into the hot zone and suspended on the balance. About 20–30 sec elapsed before the weight gain could be recorded. The design of the balance has been described elsewhere.[22] A mullite tube served as reaction chamber.

Premixed gas mixtures were continuously pumped through the apparatus during the reaction. The gas mixtures were introduced at the bottom of the reaction chamber and flowed upward past the specimen. The CO_2 and CO contents in the gas mixtures had a relative uncertainty of less than 2%. The temperature was measured inside the mullite tube next to the specimens with a Pt/Pt10%Rh thermocouple, which was protected by a closed alumina tube.

A scanning electron micrograph of a specimen surface after high-temperature annealing in high-vacuum is shown in Fig. 1. The grain boundaries which appear after the thermal etching reflect those of the γ-iron. The crystallites seen are mostly α-iron grains, emerging at the surface. X-ray diffraction studies directly on the iron surface gave well-defined lines of wüstite, showing that small amounts of wüstite were present on the surface before the oxidation was initiated. The size of the γ-iron grains in thermally etched iron surfaces was generally in the range of 30–150 μm.

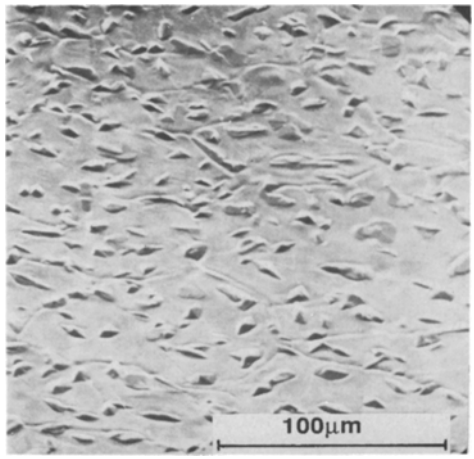

Fig. 1. SEM-micrograph of the iron surface after high-temperature annealing in high vacuum.

RESULTS

Reaction Rate Measurements

Annealed Iron

Examples of results of thermogravimetric measurements of iron in CO_2+CO mixtures at different compositions and total gas pressures at 1000°C are given in Fig. 2. Generally, the very initial behavior can be

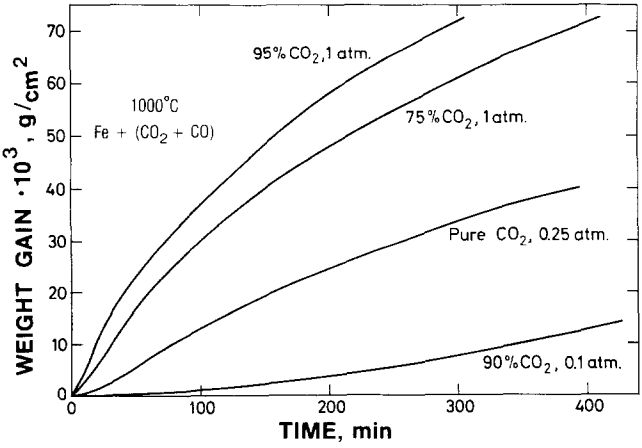

Fig. 2. Weight gain vs time for oxidation of iron in CO_2+CO gas mixtures at 1000°C.

described as nonlinear, but this tends (on further oxidation, and depending on the reaction conditions) toward a more or less linear stage. After this stage, the reaction rate increases and reaches a maximum value after which the rate again gradually decreases. In order to differentiate between different stages of the reaction, the oxide formation which takes place before the onset of the increasing reaction rates is described as "film" formation.

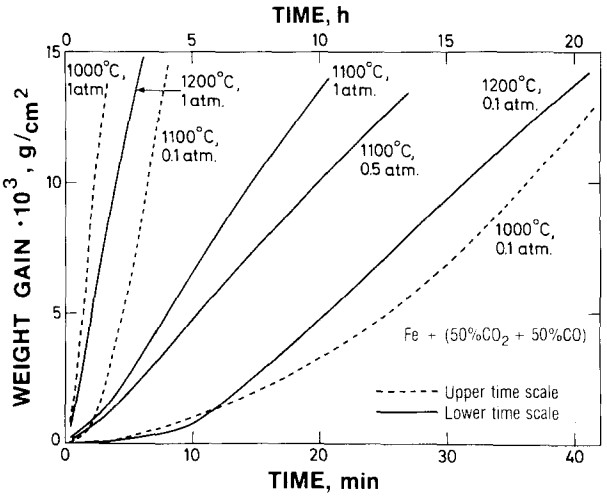

Fig. 3. Weight gain vs time for the initial oxidation of iron between 1000–1200°C in $50CO_2+50CO$ at different total gas pressures.

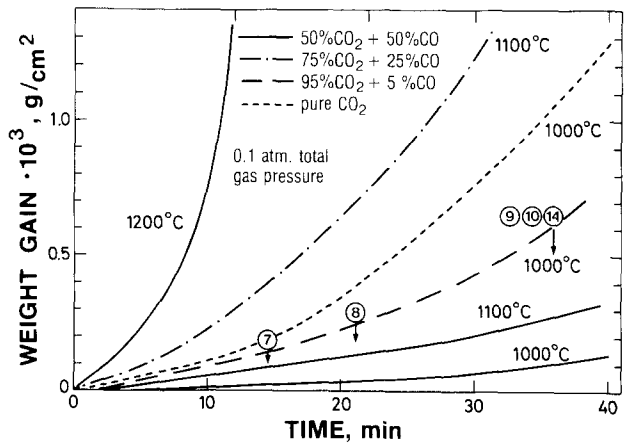

Fig. 4. Weight gain vs time for the initial oxidation of iron in CO_2+CO gas mixtures at 0.1 atm. total pressure between 1000–1200°C.

Figure 3 shows the initial oxidation behavior in $50CO_2+50CO$ at different total gas pressures. At 0.1 atm. total pressure the changes in the reaction kinetics are easily observed. All in all, a general feature of the initial oxidation is that under conditions when the reaction rates are relatively slow (e.g., at low temperatures, low total pressures, or low CO_2 content) the different stages of reaction are more clearly distinguishable than at higher reaction potentials. It may also be noted that only at 0.1 atm. total gas pressure at 1000 and 1100°C has true linear kinetics for film growth been observed in this study. This is illustrated in Fig. 4. Furthermore, film growth is generally only observed at weight gains lower than about $0.2\ mg/cm^2$.

The oxide thicknesses at which the transitions from film growth to faster rates of scale growth are larger under conditions when the reaction rates are relatively slow. This is illustrated in Fig. 5, which shows the weight

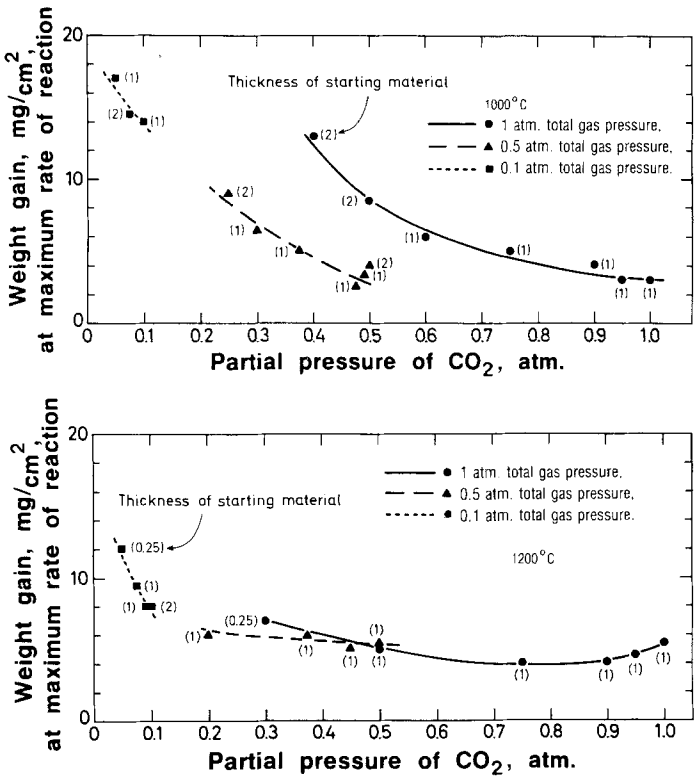

Fig. 5. (A) Weight gain at the maximum rate of reaction vs partial pressure of CO_2 at 1000°C. (B) Weight gain at the maximum rate of reaction vs partial pressure of CO_2 at 1200°C.

gains at which maximum rates of reaction are observed under different reaction conditions. As seen, the weight gain at maximum rate of reaction is larger the lower the partial pressure of CO_2. Furthermore, the region of maximum rates of reaction (in terms of weight gain) is rather narrow and takes place at weight gains ranging from 1-3 mg/cm^2. However, changes in the reaction rates may, particularly at low reaction rates, be very small for long periods of reaction. It is in these cases that linear scale growth is closely approached.

Cold-Worked Iron

Effects of cold-working the starting material were also qualitatively studied for reactions at 1000°C. This is illustrated in Fig. 6, where the reaction rates of annealed and cold-worked iron in different gas mixtures at 0.1 total gas pressure are compared. The specimens were cold-worked after the high-temperature pretreatment by hammering each side about 15 times; after this, the specimens were washed in ethanol (the specimens were protected from contamination from the hammer by a sheet of plastic).

Cold-worked materials have shorter induction periods for the start of the reactions (not revealed on Fig. 6). During a subsequent period, the reaction rates of cold-worked and annealed iron are similar, and this period becomes shorter when the reaction potential is increased. Then, during the stage with increasing reaction rate, the cold-worked materials react considerably faster than the annealed materials. The maximum rates of reaction of

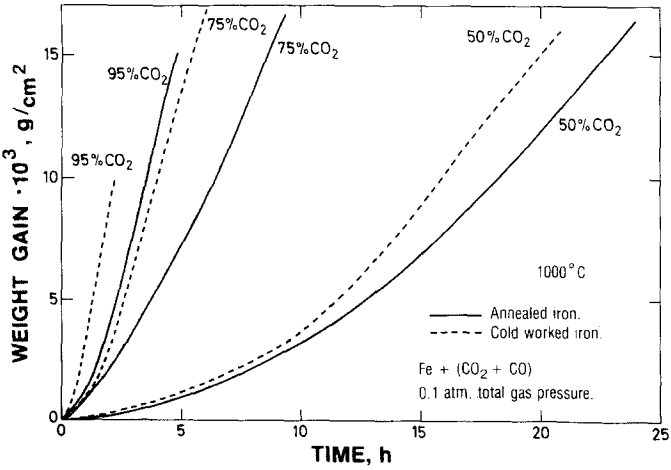

Fig. 6. Weight gain vs time for the oxidation of annealed and cold-worked iron in CO_2+CO gas mixtures at 0.1 atm. total gas pressure at 1000°C.

cold-worked materials are also higher and take place at lower weight gains compared to annealed materials.

SEM Studies

Annealed Iron

Film Growth. A number of reacted specimens were examined by scanning electron microscopy. All observations were made on quenched specimens.

After oxidation at 1000°C and 0.1 atm. total gas pressure, the scales showed a nonuniform grain structure during film growth and the subsequent stage with increasing reaction rates. These features are illustrated by micrographs (Figs. 7–10, and 14), which show surfaces of a series of specimens quenched during different stages of oxidation in $95CO_2+5CO$ at 0.1 atm. total pressure. The times of reaction at which the different specimens were quenched are shown by the arrows in Fig. 4, where the numbers refer to the different illustrations (Figs. 7–10, and 14). After 15 min of reaction, a uniform wüstite film with thickness of about 1 μm has been formed. Different surface regions are characterized by different crystal orientations. The different regions are of about the same size as the underlying γ-iron grains, and this suggests that the initially formed wüstite crystals are crystal-

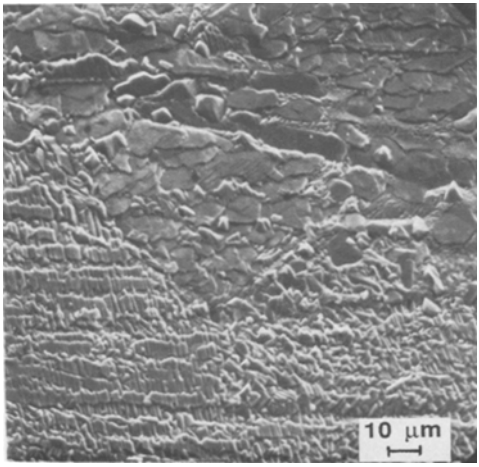

Fig. 7. SEM-micrograph showing a wüstite surface with different crystal orientations. The various crystal orientations probably reflect different orientations of the underlying iron grains.

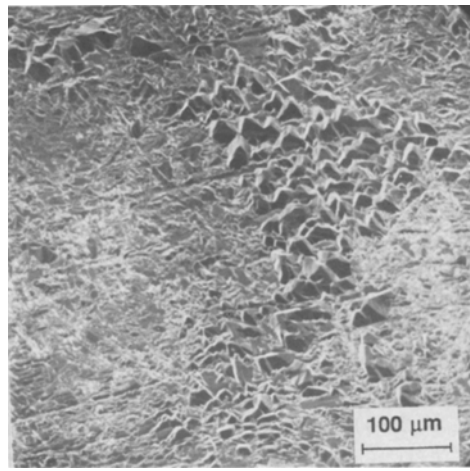

Fig. 8. SEM-micrograph showing a region of large crystals on the wüstite surface.

lographically related to the substrate, and probably grow epitaxially on the iron metal. FIgure 7 shows three regions with different crystal orientations, indicating an underlying 3-pole junction of γ-iron grains.

On further oxidation, the surface topography gradually changes. In some areas large crystals develop, while in other parts the crystal size

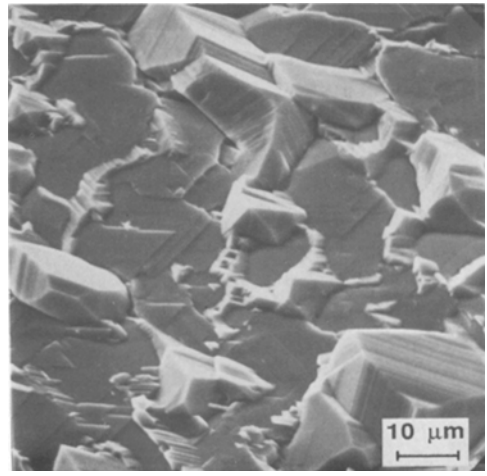

Fig. 9. SEM-micrograph showing growth of new grains on a wüstite substrate with palte-like grains.

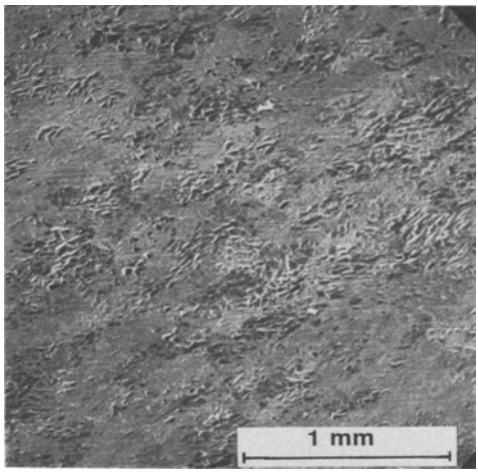

Fig. 10. SEM-micrograph of a wüstite surface with regions of different grain size.

remains essentially unchanged. This is illustrated in Fig. 8, which shows a region with large crystals, and the size of this area is similar to that of the underlying iron grain. These faster-growing crystals are faceted and macro-ledges are revealed on the crystal surfaces. Furthermore, there are no indications of formation of new oxide grains on these crystal surfaces.

At the end of the film growth, faceted grains begin to form and grow in regions where other crystal orientations dominate. This feature is demonstrated in Fig. 9 by formation of faceted grains on a wüstite substrate with plate-like grains. The nucleation appears to begin at grain boundaries, but examples have also been found where new wüstite crystals have developed on crystal surfaces. This was particularly observed at 1000°C in gas mixtures of 1 atm. total pressure with CO_2/CO ratios corresponding to those close to the $Fe/Fe_{1-\delta}O$ equilibrium.

For scales formed at 1000°C at 1 atm. total gas pressure, it was observed that during the transition from film to scale growth the areas with larger grains gradually grew until they completely covered the surface. During this transition the scales consist of wüstite grains which have different sizes. The larger grains are about 100 μm in diameter, and they probably cover single iron grains, while the smaller grains usually are less than 10 μm. This is illustrated in Fig. 10, which shows the surface of a specimen reacted to about 0.6 mg/cm^2 in $95CO_2+5CO$ at 0.1 atm. total gas pressure at 1000°C. In regions where several larger grains impinge, growth pits on the crystal surfaces may occassionally be observed during this stage. Scales formed

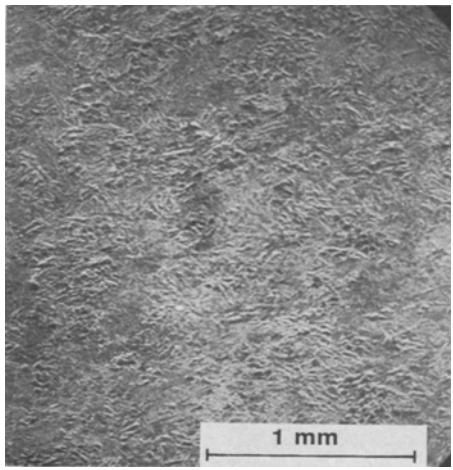

Fig. 11. SEM-micrograph of a wüstite surface with grains of nearly uniform size.

under conditions of relatively rapid reaction rates show smaller variations in grain size. Furthermore, different types of grains appear to grow, and the distribution of crystal orientations within regions of single γ-iron grains seems less uniform. These features are illustrated in Fig. 11, which shows a surface of a specimen reacted to about 0.9 mg/cm^2 at 1000°C in $95CO_2+5CO$ at 1 atm. total pressure.

Scale Growth. When large, faceted grains cover the surface, the grains have fairly uniform size, and the surface appears rough to the naked eye. On further oxidation, and particularly at higher reaction rates, numerous growth pits are also observed on the surfaces. Figure 12 shows such growth pits on a scale surface formed at 1100°C at 0.1 atm. total gas pressure in $75CO_2+25CO$ (total weight gain 30 mg/cm^2). Furthermore, smaller pits frequently condense into larger ones, and these may become visible to the naked eye. The increase in scale thickness during this stage mainly involves outward growth of the larger outer grains, which as a result also become columnar.

Scales reacted at 1000°C and 0.1 atm. total gas pressure also show another phenomena which is less typical at the other reaction conditions, and this constitutes formation of long needles and elongated sharp-edged crystals. These crystals are usually first visible near the edges of the specimens, but may after extended reactions cover the entire surface.

Studies of thick scales grown under parabolic-like kinetics and varying from about 0.5–2 mm in thickness, show that the iron/oxide interfaces

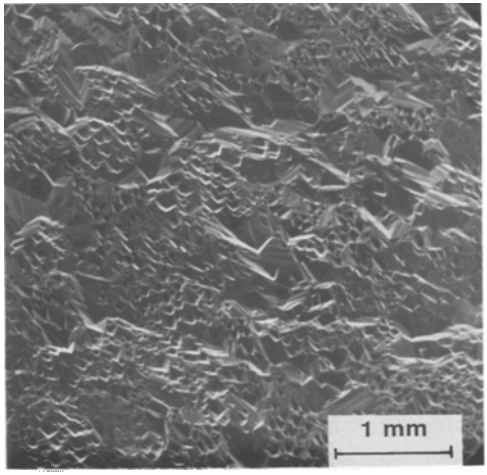

Fig. 12. SEM-micrograph of a wüstite surface with numerous growth pits.

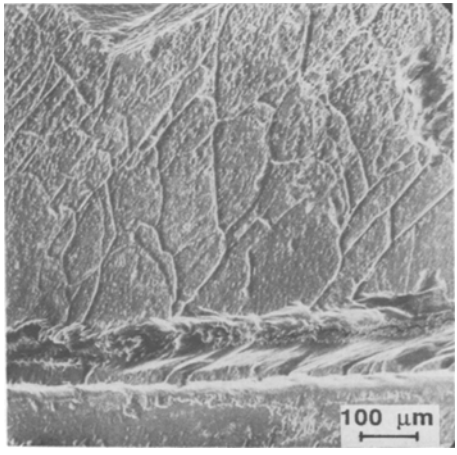

Fig. 13. SEM-micrograph showing a cross-section of the reaction product after oxidation in 0.1 atm. of a $90CO_2+10CO$ mixture at 1200°C for 70 min. A porous region is observed near the iron/wüstite interface. The iron/wüstite interface is straight and pore-free.

remain nearly straight and essentially pore-free until almost all the iron has been consumed. Scales formed at 1 atm. total gas pressure, and at high rates, particularly at 1200°C, are dense and may consist of only a few grains which extend across the entire oxide layer. For thicker scales (1–2 mm) or scales formed at reduced reaction potentials, regions of smaller grains are frequently seen near the metal/oxide interface. For these slower-growing scales, pores are usually observed in a region between the inner smaller crystals and the outer larger crystals. In this region, large cracks may be formed during cooling, and as a result the outer part of these scales occasionally spall off. Some of these features are demonstrated in Fig. 13 for a scale formed at 1200°C in $90CO_2+10CO$ at 0.1 atm. total gas pressure. The outer layer of the wüstite scale consists of columnar grains, while an inner layer contains pores and a region with smaller wüstite grains. The bottom of the micrograph shows unreacted iron and it is seen that the interface between iron and wüstite is straight and pore free.

Cold-Worked Iron

During the early stages of reaction of cold-worked iron, an oxide surface topography develops which is quite different from that described above for the annealed specimens. The wüstite grains grow in a highly anisotropic manner, and also form numerous elongated sharp-edged crystals and needles. The needles usually extend from the tip of an elongated crystal. Figure 14 shows the edge of the same specimen as illustrated in Fig. 10.

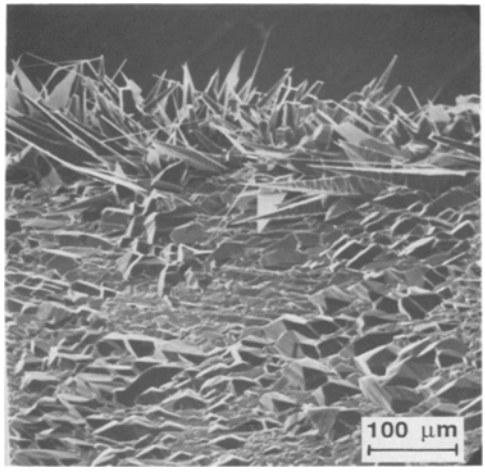

Fig. 14. SEM-micrograph of the edge of a specimen after oxidation to a weight gain of 0.6 mg/cm^2.

Since the iron specimens are cut from sheets, the edges of the specimens have been considerably cold-worked. However, the effects of this treatment on the surface topography are somewhat surprising since the iron specimens have gone through three phase transitions and a high-temperature annealing before the oxidation is initiated.

On further oxidation the differences in surface topography between cold-worked and annealed specimens become smaller and growth pits are formed. However, the grains often remain elongated and sharp, and needles may be present for substantial periods of reaction. No systematic study of the concentration of pits on annealed and cold-worked substrate were performed. However, on annealed specimens the dislocation pits usually first appear at the edges of the specimens, and, consequently, the concentration of pits is usually higher, at least during the earlier stages of oxidation, at the edges than on the faces.

DISCUSSION

Nucleation and Film Growth

The results show that for films and thin scales the nucleation of wüstite on polycrystalline γ-iron in CO_2+CO gas mixtures is crystallographically related to the underlying iron crystals. The shapes and growth rates of the initially formed wüstite crystals depend on the orientation of the metal grains. The initial reaction rate also depends on the mechanical pretreatment. Furthermore, the fact that cold-worked iron surfaces start to oxidize more rapidly on exposure to the CO_2+CO gas indicates that nucleation of wüstite is affected by this treatment. This is not surprising as nucleation probably takes place on lattice imperfections inherited from the cold-worked α-iron.

The difference in surface topography of wüstite formed on annealed and cold-worked iron indicates that the crystal growth of wüstite is considerably affected by stresses in the starting material. The elongated crystals and needles of wüstite formed on cold-worked iron suggest that the growth is favored at the tip rather than on the sides of the crystals. These growth sites may constitute screw dislocations emerging at the tip, and which continuously form new active growth sites at the tip by a spiral-type growth. For the thin scales, which are crystallographically related to the substrate, screw dislocations are probably inherited directly from the iron substrate. Furthermore, as demonstrated in Fig. 14, extensive heat treatment of the material is necessary in order to remove effects of cold-working.

Since the reaction rates of films and thin scales are controlled by a surface reaction, the higher rates of cold-worked substrates may be explained

by an increased number of active growth sites on the wüstite surface. As previously mentioned, several factors may affect the number of growth sites on the surface—for instance, the concentration of screw dislocation at the surface, scale texture, and crystal shape. As shown by the results in Fig. 6, the oxidation rates during the film growth are not markedly affected by cold-work. Thus, the dominant filamentary growth (caused by dislocations) does not immediately result in a higher overall number of active growth sites on the wüstite film surface. An explanation of this may be as follows: During the initial film growth on cold-worked iron surfaces, the oxide consists mainly of elongated crystals and needles. Since these crystals mainly grow outward at the tip, the concentration of growth sites remains nearly constant and their density is low compared to the total surface area. However, the growth rate at the tip gradually decreases as the crystals become longer, and more well-defined equaxial crystals are formed by sideways growth. This increases the overall number of growth sites on the surface and also leads to a higher number of growth sites compared to that formed on annealed materials for the same overall weight gain. This latter feature probably results from a more uniform increase in growth sites over the surface, since in cases of annealed materials reacted at these low oxidation potentials, the increase in growth sites appear mainly to depend on the increase of the surface fraction of fast-growing faceted crystals.

The strain energy and defects introduced by cold-work probably result in γ-iron grains which are much smaller than in the annealed material. This probably affects the reaction behavior, since the microstructure of the oxide film is related to the microstructure of the substrate and, as will be discussed be discussed below, microstructure and growth stress are important parameters for the initial reaction behavior.

In addition to the effects of cold-work on the mechanical properties of the substrate, impurities and dispersions of other phases may also change these properties considerably. For instance, the large effects on the initial oxidation of α-iron by small amounts of carbon (0.1–1.2 wt.%) between 600–850°C represent an interesting case.[23] Also effects of variations in grain size of the substrate on the rate of oxidation during film growth, as reported by Pettit and Wagner, could reflect changes in the mechanical properties.

Scale Growth

When scales on cold-worked substrates grow thicker, neighboring crystallites in form of elongated crystals and needles impinge, and the grain boundary areas formed are larger than in scales formed on annealed iron. Thus, if surface pits are formed in grain boundaries and migrate into the

crystals as the grains coalesce, the high concentration of these pits on wüstite surfaces formed on cold-worked substrates, as reported by Lee and Rapp,[19] could simply reflect a high density of grain boundaries. If this is correct, it seems questionable to assume that dislocations which emerge at the surface at later stages of the oxidation [and which form surface pits (or needles)] are directly inherited from the metal. Furthermore, when the scales become thicker, the crystallographic relation of the scales to the substrates disappear, and other stress-generating processes probably become more important.

Scales formed at high reaction potentials will have higher induced growth stresses than scales formed at lower rates, and in these faster-growing scales plastic deformations, creep, and grain-boundary sliding will therefore be faster, and with this, also the formation of the final (001) scale texture. These scales seem to form the final scale texture by continuous grain rotation uniformly over the scale surface. This is in contrast to scales formed at 1000°C and 0.1 atm. total gas pressure; in these cases, the scales initially consist of an inhomogeneous grain structure, where only some grains appear to grow. Here the final scale texture, which also is (001), is formed by: (i) formation of a continuous layer of large grains through grain growth in different regions of the surface, and (ii) by deformation of this grain structure by the growth stress induced when these large grains impinge. From this interpretation it is expected that the final scale texture will be reached at considerably higher scale thicknesses for scales formed at low reaction potantials.

The wüstite scale surfaces formed on cold-worked substrates at 1000°C and 0.1 atm. total gas pressure show a more uniform surface topography during the initial stages of oxidation than scales formed on annealed substrates. Furthermore, these scales consist of crystals which are generally smaller (at least in the two dimensions parallel to the surface) than the faster-growing faceted grains formed on annealed iron. Thus it appears probable that, even at low reaction rates, the final scale texture on cold-worked substrates is reached by a continuous and uniform deformation of the film. However, this process is probably initiated when the elongated crystals impinge, and this may therefore explain the late start of the rapidly increasing reaction rate for these scales. On further oxidation, these scales deform in a similar manner as scales formed at higher reaction potentials, and, as a consequence, the maximum rates of reaction are reached at lower weight gains than for scales on annealed iron. The higher maximum rates of reaction on scales formed on cold-worked iron, in particular for reactions in CO_2-rich gas mixtures, may indicate that an additional effect to the reaction rate is from screw dislocations which produce active growth sites on the scale surface. As seen in Fig. 6, this effect is reduced for very slow reactions where stress relief is larger.

Kinetics and Scale Morphology

On the basis of the above results and discussion, a general model relating kinetics and scale morphology may be formulated. Let us first consider reactions at very low reaction potentials. The initial nonlinear film growth reflects the nucleation and growth of wüstite and gradual formation of a wüstite film of nearly uniform thickness and which is crystallographically related to the underlying iron substrate. The subsequent linear film growth reflects mainly the growth of crystals with a preferred orientation, and which vary depending on the orientation of the substrate metal. During this linear film growth the number of active growth sites is essentially constant and is determined by the texture of the film.

The transition from film growth to a more rapid scale growth is initiated when faster-growing grains expand to neighboring regions on the surface (where they are not crystallographically related to the iron substrate). The increase in oxidation rate suggests that this change in crystal orientation enhances the rate of the surface reaction. The final orientation of these crystals is probably close to that of the final scale texture, where (001) planes are parallel to the iron surface. Since the reaction is essentially limited by the rate of the surface reaction under these conditions, it is concluded that these fast-growing crystals have higher concentrations of growth sites on the crystal surfaces.

Scales formed at high reaction potentials show more uniform grain structures during the first stages of oxidation. Due to the more homogeneous microstructure and larger growth stresses which are produced in these faster-growing scales, the scale texture is gradually changed through continuous deformation of the wüstite film. A stable film texture is never obtained (as for slow reacting scales) and as a result, a linear film growth is not observed. Rather, the surface texture of fast-reacting scales change continuously, and film and scale growths overlap.

The maximum rate of oxidation represents a competition between (a) an increasing rate of reaction due to an increasing number of growth sites which results from the change in surface texture of the scale and (b) a decreasing rate of reaction due to a decreasing rate of diffusion of iron through the growing scale. The region with maximum rate has often been termed linear scale growth.

According to this interpretation, the final scale texture is expected to be approached at lower weight gains for the higher reaction potentials, since the growth stresses increase with the rate of reaction, in general accord with the results in Fig. 5.

During the transition to a decreasing reaction rate, the final texture is approached, and the number of reaction sites may then reach a steady-state

value. The outer grains now grow preferentially outward and become elongated. This is probably a result of compressive growth stress induced by the retarding iron/oxide interfase. The fact that scales formed at high temperatures in gas mixtures with high CO_2 contents occasionally consist of grains which extend through the entire scales, indicate that only grains in the region close to the oxide/iron interface undergo recrystallization due to growth stress. In cases of slower oxidation (i.e., under conditions of reduced reaction potentials or when scales become very thick), stresses are to a larger extent relieved during the reaction, and this may subsequently allow for a certain growth of crystals near the iron/oxide interphase. Pores may be observed in the region between outer larger grains and inner smaller grains in these latter cases, and this probably reflects a lower ability of these grain structures, which have larger inner grains, to deform when the iron/oxide interface retreats. When the number of pores increases, the effective cross-sectional area for diffusion decreases, and this leads to a reduction in the oxidation rate. Figure 15 shows two examples of such deviations from parabolic reaction behavior. As shown, the rate of reaction of a specimen oxidized in $50CO_2+50CO$ at 0.1 atm. total gas pressure at 1000°C deviates from parabolic reaction behavior after extended oxidation, while a speciment reacted in the same gas mixture, but at 1 atm. total gas pressure, shows no deviation at corresponding weight gain.

The course of oxidation of iron in CO_2+CO gas mixtures may be summarized by the graph given in Fig. 16. In this figure different stages and

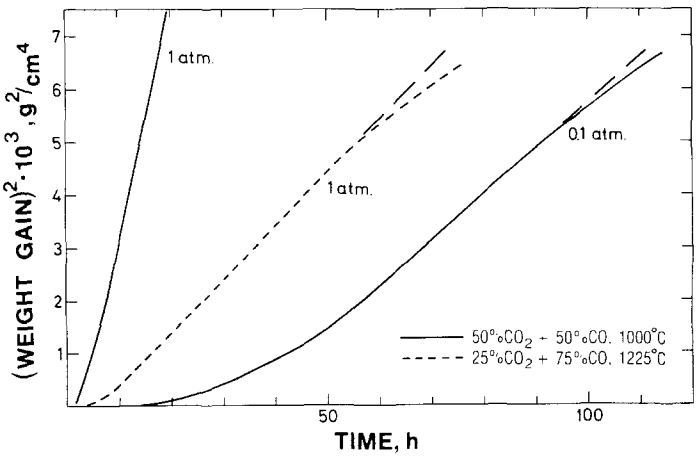

Fig. 15. Parabolic plots [(weight gain)^{2}vs time] for oxidation of iron in CO_2+CO gas mixtures under various reaction conditions. After extended reaction a deviation from parabolic behavior is observed for slow-reacting specimens.

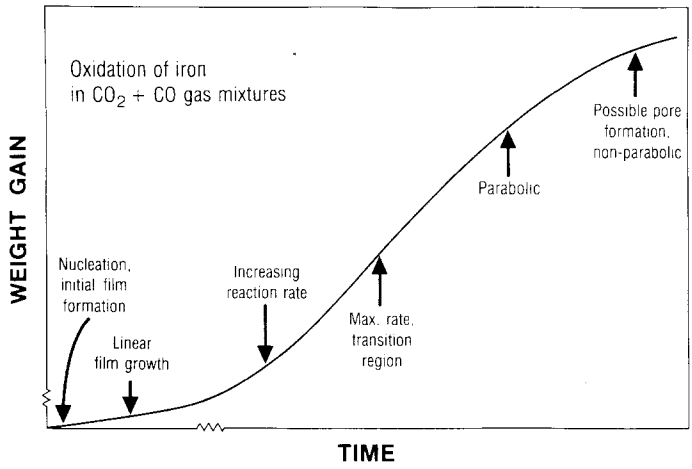

Fig. 16. Schematic illustration of the oxidation kinetics of iron in CO_2+CO gas mixtures.

some characteristic features are indicated. As explained above, the relative durations of the different stages depends on temperature, CO_2 content, and total ambient gas pressure.

REFERENCES

1. K. Hauffe and H. Pfeiffer, *Z. Metallk.* **44**, 27 (1953).
2. W. W. Smeltzer, *Trans. Met. Soc. AIME* **218**, 674 (1960).
3. W. W. Smeltzer, *Acta Met.* **8**, 377 (1960).
4. F. S. Pettit, R. Yinger, and J. B. Wagner, Jr., *Acta Met.* **8**, 617 (1960).
5. F. S. Pettit and J. B. Wagner, Jr., *Acta Met.* **12**, 35 (1964).
6. K. Hedden and G. Lehmann, *Arch. Eisenhüttenwesen* **35**, 839 (1964).
7. E. T. Turkdogan, W. M. McKewan, and L. Zwell, *J. Phys. Chem.* **69**, 327 (1965).
8. L. A. Morris and W. W. Smeltzer, *Acta Met.* **15**, 1591 (1967).
9. E. T. Turkdogan and J. V. Vinters, *Met. Trans.* **3**, 1561 (1972).
10. S. M. El Raghy, F. Jeannot, and C. Gleitzer, *J. Mater. Sci. Lett.* **13**, 2510 (1978).
11. F. Nardou, P. Raynoud, and M. Billy, *J. Chim. Phys.* **76**, 595 (1979).
12. H. J. Grabke, *Ber. Bunsenges. Phys. Chem.* **69**, 48 (1965).
13. H. J. Grabke and H. Viefhaus, *Ber. Bunsenges. Phys. Chem.* **84**, 152 (1980).
14. H. J. Grabke and H. Viefhaus, *Mater. Sci. Monographs (Reactivity of Solids)* **10**, 410 (1982).
15. J. Bardolle and L. Bérnard, *Rev. Met.* **49**, 613 (1952).
16. J. Bardolle, *Rev. Met.* **51**, 833 (1954).
17. E. A. Gulbransen, W. R. McMillan, and K. F. Andrew, *Trans. AIME* **200**, 1027 (1954).
18. E. A. Gulbransen and K. F. Andrew, *J. Electrochem. Soc.* **106**, 511 (1959).
19. M. Lee and R. A. Rapp, *Oxid. Met.* **27**, 187 (1987).
20. T. I. Jungling and R. A. Rapp, in *Proc. High-Temp. Mater. Chem. II* Z. A. Munir and D. Cubiciotti, eds. (Electrochem. Soc., Pennington, New Jersey, May 1983), pp. 199-208.
21. L. E. Matson, H. Erhart, M. Lee, and R. A. Rapp, *Met. Trans. A* **15A**, 2241 (1984).
22. K. Holthe and P. Kofstad, *Corrosion Sci.* **20**, 919 (1980).
23. A. U. Malik and D. P. Whittle, *Oxid. Met.* **16**, 339 (1981).